ČESKÉ VYSOKÉ UČENÍ TECHNICKÉ V PRAZE

Fakulta Jaderná a Fyzikálně Inženýrská

BAKALÁŘSKÁ PRÁCE

2006 **Radek Šmakal**

CZECH TECHNICAL UNIVERSITY IN PRAGUE

Faculty of Nuclear Sciences and Physical Engineering

Department of Physics

Silicon drift detectors of the inner tracking system (ITS) of the ALICE experiment at LHC

(Křemíkové driftové detektory vnitřního dráhového systému (ITS) experimentu ALICE na urychlovači LHC)

Bachelor's Thesis

Author: Radek Šmakal
Supervisor: RNDr. Vojtěch Petráček CSc.

Academic year: 2005/2006

Silicon drift detectors of the inner tracking system (ITS) of the ALICE experiment at LHC
(summary)

This bachelor's degree project summarizes the design of the ALICE experiment, with special view to silicon drift detectors of the inner tracking system. It also offers overview of processes in the semiconductor detectors (mainly silicon detectors) and explains principle of the silicon drift detectors, both with linear and radial drift geometry.
Keywords: experiment ALICE, ITS, SDD, silicon drift detector

Křemíkové driftové detektory vnitřního dráhového systému (ITS) experimentu ALICE na urychlovači LHC
(abstrakt)

Tato bakalářská práce shrnuje konstrukci experimentu ALICE, se speciálním zaměřením na křemíkové driftové detektory vnitřního dráhového systému. Poskytuje také potřebný přehled dějů v polovodičových detektorech (zejména křemíkových) a vysvětluje princip křemíkových driftových detektorů, a to jak detektorů lineárních, tak i detektorů s radiálním driftem.
Klíčová slova: experiment ALICE, ITS, SDD, křemíkový driftový detektor

Prohlášení

Prohlašuji, že jsem svou bakalářskou práci vypracoval samostatně a použil jsem pouze podklady (literaturu, projekty, SW atd.) uvedené v přiloženém seznamu.

Nemám závažný důvod proti použití tohoto školního díla ve smyslu § 60 Zákona č.121/2000 Sb., o právu autorském, o právech souvisejících s právem autorským a o změně některých zákonů (autorský zákon).

V Praze dne 7.6.2006 Radek Šmakal

Acknowledgements:

I would like to thank to RNDr. Vojtěch Petráček CSc. for his professional assistance and remarks, Mr. Klaus Hitschler for his advices about his software and Bc. Tomáš Valenta for the language and typographical remarks and for his font Atomino.

Table of contents

Introduction

I chose the topic of this Bachelor's Degree Project for several reasons. I wanted to learn about modern particle detection systems, obtain information about ALICE and heavy-ion collisions, but above all, I wanted to be acquainted with electronics used in the experimental particle physics. This bachelor's degree work is written in English due to the fact that English is the main language in the scientific community, availability of the English sources related to this topic, and also because of exercising motivation. The main topic of this text is a silicon drift detector (SDD) which will be used in ALICE. Therefore, I familiarized the reader with ALICE and focused especially on its inner tracking system, because SDDs are optimized for use in ITS and its construction must be chosen considering the other detectors in complex. I tried not simply write the attributes of the detectors, but to contextualize them.

The introductory part of this bachelor's degree work discusses semiconductor detectors (almost exclusive silicon semiconductor detectors) from the point of view of properties of the suitable material, behaviour of charge carriers (electrons and holes), general principles, and properties.

The second part studies silicon drift detectors, both with linear and radial geometry. This part includes general principles, advantages and disadvantages.

The third part offers overview of the detector complex ALICE and involved subdetectors. It also contains motivation for constructing such sophisticated device. From this part, the abbreviation SDD will be used only for the linear silicon drift detector developed for ALICE.

The fourth part deals with parameters of the inner tracking system and two of its three subdetectors - silicon pixel detector and silicon microstrip detector.

In the fifth part, the reader is familiarized with the design and properties of the silicon drift detector developed for ALICE, with placement, prototype test results, electronics, trigger, cabling, data reduction and cooling.

The closing sixth part includes information about my work on PCI-VME interface. It was my part of the work at the apparatus for testing SDDs.

Chapter 1

Semiconductor detectors

1.1 Construction material

Development of semiconductor components require humungous investments, both financial and technological, so development of semiconductor detectors started after establishing the technological base. Production of semiconductor detectors would never pay invested costs. Area of interest changed rapidly from the Ge semiconductors to Si, where can be complex integrated circuits (for example microprocessors) mass produced. Germanium is suitable for detection of photons thanks to its great proton number (Z = 32), so the development of the germanium semiconductor detectors began later, too. Silicon (Z = 14) is used for production of detectors for low energy photons and charged particles.

1.2 Mean energy for creation of electron-hole pair

Semiconductors have a small width of forbidden band, of the order from tenths to ones eV. For this reason, mean energy for creation of electron-hole pair for Si and Ge is around 3eV. This energy depends on temperature and kind of semiconductor material and very little (less then 3%) on kind of radiation. Gaseous detectors have $w \approx 30eV/pair$ and then arise 10x more charge carriers in semiconductor detectors than in gaseous. Electron-hole pairs are created in semiconductor detectors thanks to radiation; separation of those is necessary, or else they recombine. This is possible owing to their drift in electric field.

Motion of charge carriers is caused by several effects: heat motion, drift in electrical and magnetic field and diffusion.

1.3 Drift in electrical field

Drift velocity of electrons and holes is similar (in comparison with gas detectors, where speed of electrons is thousand times greater then velocity of positively charged ions). For relatively low electrical field ($E \leq 10^4 Vm^{-1}$) is drift velocity linear function of the field:

$$\begin{aligned} \vec{v_e} &= -\mu_e \vec{E} \\ \vec{v_h} &= +\mu_h \vec{E} \end{aligned} \tag{1.1}$$

where v_e, v_h is drift velocity of electrons and holes, E is intensity of electrical field and μ_e, μ_h are mobilities of electrons and holes. Mobilities depend on a kind of semiconductor and on the temperature. When the temperature is higher, mobility is lower (thanks to scattering on lattice).

Material		Si	Ge	GaAs	InSb	SiC	diamond
Mobility	e	0.13	0.45	0.88	7.70	0.01	0.18
$m^2V^{-1}s^{-1}$	h	0.05	0.35	0.04	0.075	0.005	0.12

Table 1.1: *Mobilities of selected materials (at 300K).*

The conductivity of material is caused by both electrons and holes, so we can write:

$$\sigma = ne\mu_e + pe\mu_h \tag{1.2}$$

where n is concentration of electrons and p is concentration of holes. In electrical fields $10^4 Vm^{-1} \leq E \leq 10^5 Vm^{-1}$, v_e and v_h are growing slower, and after reaching a saturated velocity ($E \approx 10^5$–$10^6 Vm^{-1}$) are independent of further growing of E. Saturated velocity is almost the same for electrons and holes, and also for Si and Ge. Its value is approximately $10^5 ms^{-1}$ (almost independent of the temperature). Many detectors work with saturated drift velocity. For the detector width 1mm is a time of charge collecting about $10^{-8}s$ and shorter, so the silicon detectors are one of the detectors with the fastest response.

1.4 Diffusion

If the charge isn't distributed in the material evenly, it is moving from the area of higher concentration to the area of lower concentration. Diffusion flux density is:

$$\begin{aligned} \vec{J}_e^{(DIF)} &= +eD_e\nabla n \\ \vec{J}_h^{(DIF)} &= -eD_h\nabla p \end{aligned} \tag{1.3}$$

where D_e, D_h are diffusion constants for electrons and holes. The total flux density for electrons (drift and diffusion merged) can be written as:

$$\vec{J}_e(\vec{r}) = e[n(\vec{r})\mu_e\vec{E}(\vec{r}) + D_e\nabla n(\vec{r})] \tag{1.4}$$

and from this equation is possible to obtain [1] the Einstein expression:

$$\mu_e = \frac{e}{kT}D_e \tag{1.5}$$

which connects diffusion constant and mobility (for holes can be obtained similar expression).

1.5 Motion in the magnetic field

Semiconductor detectors are less sensitive to the magnetic field than, e.g., photomultipliers. Yet, it is necessary to pay attention to some phenomena.
In the magnetic field, particle (electron, hole) is affected by the Lorentz force:

$$\vec{F} = q(\vec{E} + \vec{v} \times \vec{B}) \tag{1.6}$$

Analysis for the silicon drift detectors can be found in [7].

1.6 Creation of charge carriers

Three different processes are involved in creation of charge carriers: thermal generation, optical excitation and ionization by charged particles. Last two will be briefly described in the next section (1.8). Thermal generation is an undesirable process, because it magnifies the noise. This is the reason why Ge semiconductors must be maintained at low temperature. This is not necessary for Si and GaAs semiconductors.

1.7 Spatial distribution of the charge

- UV, visible light - energy suffice for only one electron-hole pair, it arises in surface region (far less than $1\mu m$ deep)
- x-ray, γ - this is point interaction, with many created electron-hole pairs
- α-particles - length of track is several μm, distribution is according to Bragg's curve (maximum of deposited energy is at the end of track)
- β-particles - less energy losses and longer tracks, in comparison with α-particles
- high-energy charged particles - uniform distribution of the energy, total deposited energy is proportional to Z^2 (Z of the particle)
- non-relativistic charged particles - energy losses proportional to $1/E$ and Z^2, particle identification[1] is possible due to measuring with two detectors

1.8 Recombination

Electrons and holes in semiconductor can directly recombine with each other; it is characterized by mean lifetime. In the intrinsic semiconductors, due to residual admixtures, the average value of mean lifetime is from $10^{-3}s$ to $10^{-4}s$. Theoretically, in perfectly pure semiconductor, the mean lifetime is around 1s. The difference is caused by impurities, which create so-called recombination centers, with energy levels near to the center of the forbidden band. These centers are similar to catalysts in chemistry. E.g., recombination center catches electron from conducting band. Later, it catches a hole from valence band, electron fill the hole, recombination center gets itself to the initial state and is ready for the next recombination process. Other impurities, mainly metals as Au, Cd or Zn, occupy node points of the crystal lattice and form so-called traps, also with energy levels near to the center of the

[1] Two detectors are usually used - transit detector (where particle abandons only a little of energy) and absorptive detector (where particle stops). For ionization losses is valid (Bethe's equation):

$$\frac{dE}{dx} = C_1 \frac{mZ^2}{E} \ln C_2 \frac{E}{m} \tag{1.7}$$

after simply modification we get:

$$E\frac{dE}{dx} = C_1 mZ^2 \ln C_2 \frac{E}{m} \propto Z^2 \tag{1.8}$$

This equation can be used as a criterion for particle identification.

forbidden band. Charge carriers can be imprisoned in these traps for relatively long time so they can't drift through crystal. Even if trap releases it's victim and charge carrier can return to drifting through crystal, it can be too late for contribution to signal. The result is amplitude effect and noise. In summary, purity of the semiconductor is very important for construction of semiconductor detectors (we need the mean lifetime in order of $10^{-5}s$ and longer).

Semiconductor detectors are realized by p-n junction. Junction from one kind of semiconductor to another must be accomplished without disruption of crystal lattice, thus it is not possible simply put on two different semiconductor lattices together. I don't want to write about possibilities of realization p-n junctions, this is not necessary for explication of drift detectors for ALICE.

Semiconductor junction behaves like a diode and can be polarized in the inverse direction. Majority of charge carriers can't drift through the junction and are sucked off from junction neighborhood. There arises area without free charge carriers (depleted area), suitable for detection. Electrons and holes, created when particles interact in this area, migrate in the field and make a current (charge) signal. From the point of view of the minority charge carriers, junction polarized in the inverse direction acts like an oriented in the conducting direction, amplitude of the current in such junction is proportional to the densities of minority charge carriers in both parts of the junction. In application, one part of the crystal is usually much more doped than the part of the opposite type of conductivity. Generally, expression of the thickness of the depleted area [10] can be written in the form:

$$l = \sqrt{\frac{2\varepsilon_r\varepsilon_0 U}{eN}} \tag{1.9}$$

where N is a volume density of the doping elements and U is the inverse voltage on the junction. Better measurable than N is a resistivity r_D of the less doped part of the semiconductor. r_D can be expressed as:

$$r_D = \frac{1}{e\mu N} \tag{1.10}$$

where μ is a mobility of the majority charge carriers. Merging these two equations, we get the most frequently written expression for active thickness of the semiconductor detector:

$$l \approx \sqrt{2\varepsilon_r\epsilon_0 U r_D} \tag{1.11}$$

We demand the thickest depleted area of the same voltage. According to the expression (1.11), for the maximal thickness we need the detector made from the material with very high value of the resistivity. The resistivity is limited by the purity of the basic material. The highest purity of the basic material is the main requirement for the production of the quality detectors. Depleted area behaves like a capacitor with the distance between electrodes l. Its capacitance is:

$$C = \frac{S\epsilon_r\epsilon_0}{l} \approx S\sqrt{\frac{e\epsilon_r\epsilon_0 N}{2U}} \tag{1.12}$$

where S is a junction area. For the minimal electronic noise (and so the better energetic resolution) is advantageous the lowest capacitance of the detector (due to the charge sensitive preamplifiers). According to the expression (1.12), reaching the lowest capacitance is possible for the high supply voltage of the detector.

1.9 Maximum operational voltage, breakdown voltage

The value of the voltage is limited by the so-called breakdown voltage. If the intensity of the electric field exceeds the critical value (order of the $10^7 Vm^{-1}$), breakdown occurs and the detector is destroyed. Breakdown voltage can be found experimentally by destroying the detector. Maximal operational voltage of the detector is possible to obtain from the volt-ampere dependence (beginning of the sudden grow of the current). Maximum operational intensity of the electric field must not be exceeded.

Chapter 2

Silicon drift detectors

2.1 Principle

Silicon drift detectors were invented in 1984 by E. Gatti and Pavel Řehák. First functional prototypes: Gatti, Řehák, Kemmer, Luty - Munich 1985.

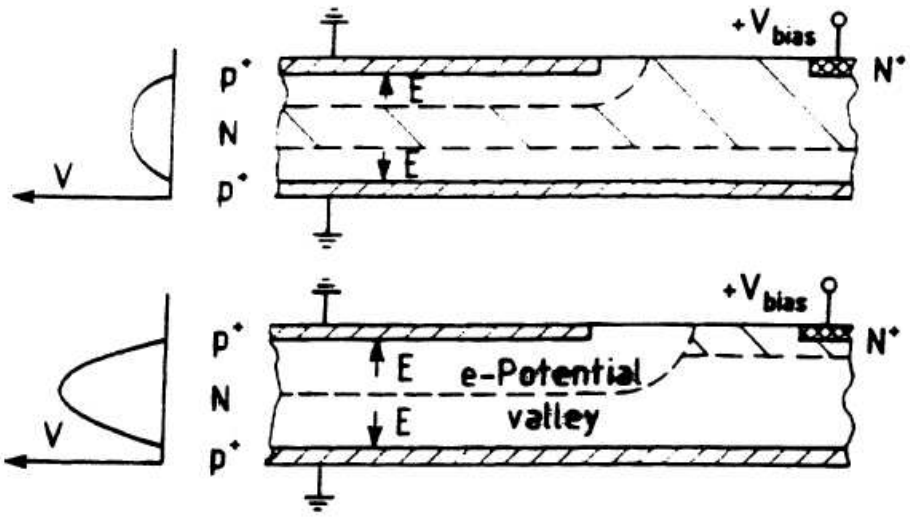

Figure 2.1: *Basic structures of the SDD. Double-diode partially (top) and fully (bottom) depleted.*

Basic structures of the SDD are shown in Fig. 2.1. If the voltage is low, both depleted areas are fully separated, but they join into one area with high voltage and a potential valley for the electrons arises in the middle of the detector. Creation of the depleted area from both sides is advantageous, because, according to the expression (1.11), we need four times lower voltage. Better attributes can be obtained by separating the p^+ area into strips (Fig. 2.2). On these strips arise the potential gradient, which leads electrons to the anode. Shape of the field depends on the geometry of the individual electrodes. Measurement of the charged particle position is possible thanks to the measurement of the drift time. Drift detectors have great advantage against strip detectors - much less number of channels. On the other hand, the disadvantage is the low speed (processing of the signal, which arrives during the processing of the previous signal is difficult and ambiguous).

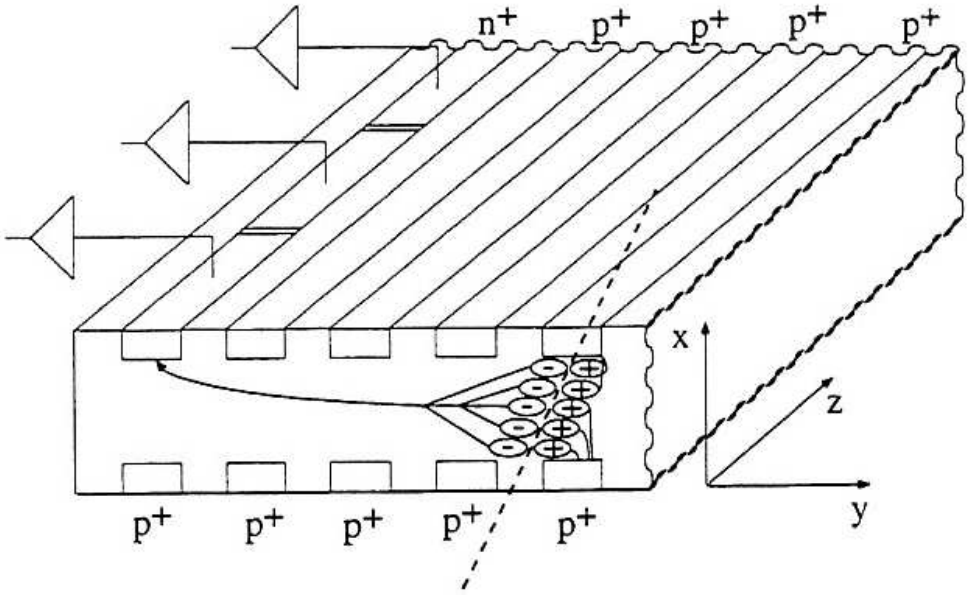

Figure 2.2: *Principle of the linear silicon drift detector with strips.*

2.2 Linear drift detectors

Many difficulties uncover during the practical realization of the drift detectors. Requirement of the gradually escalating voltage on p^+ strips leads to the very high voltage on the last strips (up to kilovolts). It is necessary to care for the ends of strips and use guarding structures in order to prevent the breakdown. The geometry of the real detector is then relatively difficult. Two dimensional measurement of the particle position can be realized by the segmentation of the anode to small segments.

2.3 Radial drift detectors

Another used geometry is a radial geometry (Fig. 2.3). It permits simpler construction, because it is not necessary to close individual p^+ strips carefully. Thanks to the small anode (and thus small capacitance), this detector offers very low noise. This is the reason why it is often used in the spectroscopy. One of the other setups is one-sided - the bottom side has a continuous coat of the implant. The advantage of this solution is a homogenous content of the material for the low penetrating radiation. 2-D resolution can also be reached by the separation of the anode (then it will measure r and φ).

In this place I mention detector called AZTEC [8], because it relates with practical part of this thesis. AZTEC is a large area cylindrical silicon drift detector ($55cm^2$) for charged particles, designed for the NA45/CERES and WA98 experiments. Electrons drift radially from the center towards the outside, where are collected by 360 anodes. Each anode is subdivided into five segments, which are interlaced with the neighboring anodes (total number of read

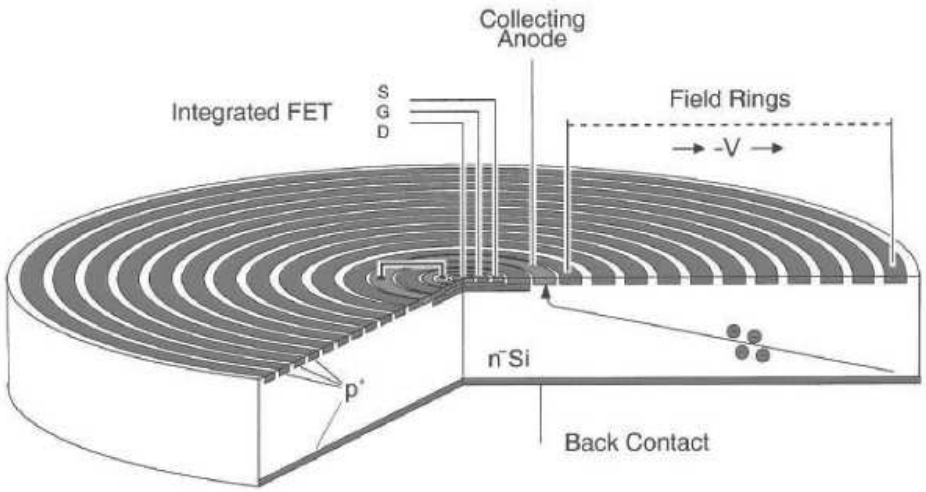

Figure 2.3: *Radial drift detector for X-ray spectroscopy with point anode and embedded electronics.*

out channels is 720). With this geometry and typical operating voltage, the maximum drift time is less than $4\mu s$. The drift velocity is monitored by measuring the drift time of electrons injected at 48 injection points.

2.4 Spiral drift detectors

Spiral x-ray detector [9] is an improvement of the cylindrical detector. The concentric rings are replaced by a continuous spiral, which leads electrons towards the anode placed in the center. The spiral geometry design leads to a decrease of the detector leakage current and the very small capacitance of the anode ($60fF$). The spiral detector operating at room temperature has a resolution comparable with cooled semiconductor detectors.

2.5 Resolution

Position resolution of the drift detectors is determined by the time resolution, i.e., by the precision of the measurement maximum of the pulse. Inaccuracy is caused by:

- signal widening (repulsion of the electrons, diffusion [5]) - it depends on the position of the interaction
- leakage current - characteristic of the detector, it can be affected by the temperature

Chapter 3

ALICE

3.1 Overview

In this part I briefly describe a detector complex ALICE. Each detector is optimized for particular experiment and its construction must be chosen considering the other detectors in complex. Amount of matter, proportions, sort of cooling, power supply, cost, and other attributes must be taken into consideration.

ALICE [2] will study the phase transition from ordinary nuclear matter to a plasma of deconfined quarks and gluons, as it is believed to had existed when the universe was just a few μs old (in time $10^{-5}s$ was size of the universe about 3km and typical temperature was higher than 150MeV) and which might still play a role in the core of collapsing neutron stars.

ALICE was first proposed as a central detector in 1993 and later complemented by an additional forward muon spectrometer (designed in 1995). It is a general-purpose heavy-ion experiment, sensitive to the majority of known observables (including hadrons, electrons, muons and photons). ALICE will measure the flavor content and phase-space distribution, event by event, for a large number of particles whose momenta and masses are typical for the temperature of 200MeV. The experiment is designed to handle the highest particle multiplicities anticipated for Pb-Pb collisions ($dN_{ch}/dy = 8000$). In addition to heavy-ion collisions, the ALICE Collaboration will study also collisions of lower-mass ions and protons (both p-p and p-nucleus), which provide reference data for the nucleus-nucleus collisions.

The average event-rate for Pb-Pb collisions at the LHC will be of the order of 10^4 minimum-bias collisions per second. Of these, approximately 100 events/s correspond to the most interesting central collisions with maximum particle production. These rates are matched with the dead-time of the slowest detector and the capabilities of DAQ system. Running times of ALICE for heavy-ion collisions are estimated on $10^6 s/year$ ($\sim$ 10% of the total) at luminosity $5 \times 10^{26} cm^{-2} s^{-1}$, yielding 10^7 central events collected for offline analysis. The overall detector layout of the ALICE experiment is shown in Fig. 3.1.

The central part is embedded in a large magnet with a weak solenoidal field. It consists (from the inside out) of an Inner Tracking System (ITS) with six layers of high-resolution silicon detectors, a cylindrical Time Projection Chamber (TPC) and a large area PID array. There is also a forward muon spectrometer and small area single-arm detector: an electromagnetic calorimeter (PHOS). The set-up is completed by a set of Zero-Degree Calorimeters (ZDCs)

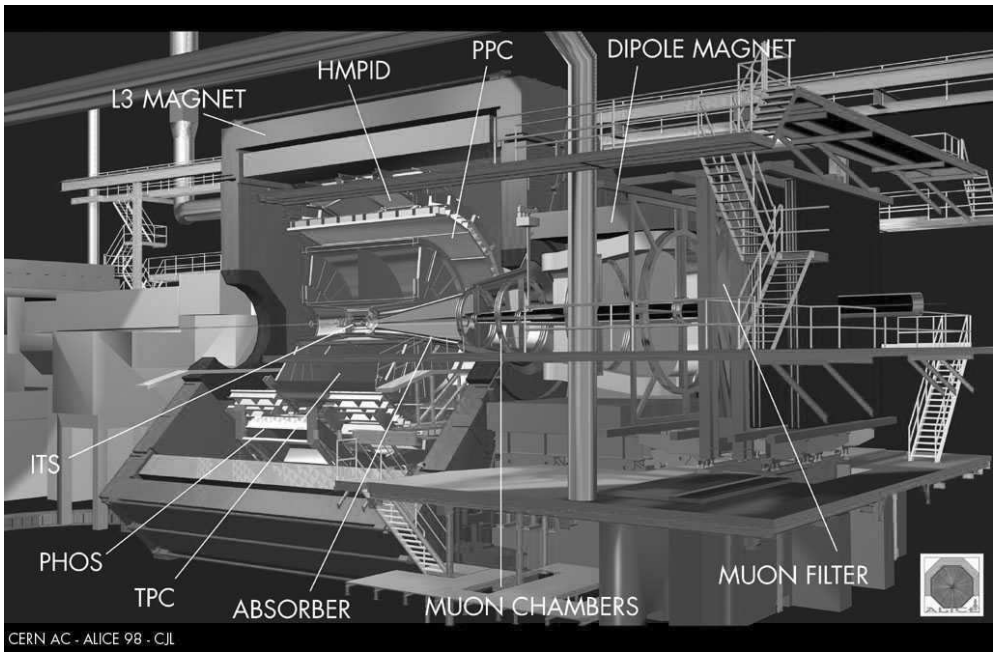

Figure 3.1: *Layout of the ALICE detector*

located far downstream in the machine tunnel, a Forward Multiplicity Detector (FMD) and a Photon Multiplicity Detector (PMD).

3.2 Magnet

The magnet of the L3 experiment at LEP will be used; it fulfils all requirements. The field strength is 0.4T (a compromise between momentum resolution, low momentum acceptance and tracking efficiency).

3.3 Inner tracking system

This is the innermost layer of the detector. The basic functions of the ITS are secondary vertex reconstruction of charm and hyperon decays, particle identification and tracking of low-momentum particles. These functions are achieved with six barrels of high-resolution silicon detectors. The ITS is made only from silicon detectors, which promise similar requirements in the terms of services, cooling and mechanics. The number of layers and their position has been optimized for cost, efficient pattern recognition and impact parameter resolution. Because of high particle density, the four innermost layers must be truly two-dimensional (silicon pixel and silicon drift detectors). Two outer layers will be equipped with double-sided silicon micro-strip detectors. Silicon drift and silicon strip layers have analog readout for independent particle identification via dE/dx in the non-relativistic region, so it can serve as a low-p_t particle spectrometer.

3.4 Time projection chamber

TPC surrounds the ITS and serves as the main tracking system. The TPC is a gas-filled ($88m^3$ of Ne/CO_2, 90%/10%) detector with an electric field applied across it. Electrons liberated by ionization of the gas, caused by a passing charged particle, drift in the electric field and are detected at the end of the chamber. The inner radius of the TPC (r $\approx$ 90cm) is given by the maximum acceptable hit density ($0.1cm^{-2}$), the outer radius (250cm) is determined by the length required for a dE/dx resolution.

3.5 Transition radiation detector

TRD is placed around TPC and will be used to identify electrons and positrons. It means, e.g., pairs directly produced in the initial stages of the collision or pairs produced as the result of the decays of heavier particles. The TRD, in conjunction with the ITS and TPC, will be able to identify the sources of electron-positron pairs. TRD will measure the radiation emitted when charged particles cross the boundary between two media with different indices of refraction.

3.6 Particle identification system

There are two detector systems dedicated exclusively to PID - a Time Of Flight (TOF) array optimized for large acceptance and average momenta and a small system specialized on higher momenta (HMPID).

3.7 Photon spectrometer

Single-arm high-resolution electromagnetic calorimeter, which can measure prompt[1] photons, π^0's and η's. It is located 5m from the vertex and consists of $PbWO_4$ scintillating crystals. In order to increase the light output, the detector will be cooled to -25^oC .

3.8 Forward muon spectrometer

Forward muon arm is designed to cover the complete spectrum of heavy quark resonances as J/Ψ, Ψ', Υ, Υ' and Υ". It will measure the decay of these resonances, both in p-p and in heavy-ion collisions. The first section of the spectrometer is a composite absorber, one meter from the vertex, made from layers of both high and low Z materials to reduce multiple scattering and particle leakage. The composite absorber is followed by a large dipole magnet (3Tm field integral), placed outside the L3 magnet, and 10 planes of thin high-granularity tracking stations. Second absorber (iron) at the end of the spectrometer and two more tracking planes are used for muon identification and triggering. The spectrometer is shielded by

[1]Prompt photons come directly from the collision and can reveal the characteristic thermal radiation from the quark-gluon plasma.

a dense tungsten tube, which surrounds the beam pipe.

3.9 Forward detectors

- Two sets of ZDCs will be used for detection of spectator[2] nucleons. They are placed 116m from the interaction point, on both sides. ZDC is made of tungsten and lead with embedded quartz fibres.
- The PMD is located 360cm from the interaction point, on the opposite side of the forward muon spectrometer.
- The FMD consists of five silicon-strip ring counters placed on both sides of the interaction region.
- The V0 detector is made of two scintillator arrays located asymmetrically on each side of the interaction point (at 355cm and -90cm).
- The T0 detector consists of two arrays of Cherenkov counters. They are placed on both sides of the interaction point, 350cm and -70cm from the interaction area.

[2]spectators are non-interacting beam nucleons

Chapter 4

ITS

4.1 Overview

ITS (Fig. 4.1) is a central part of the ALICE, closest to the beam pipe. The main functions of ITS [3] are: finding of the primary and secondary vertices, track finding and particle identification of low-p_t particles and support for the TPC (momentum and angle measurements).The ITS consists of six cylindrical layers of silicon detectors (similar requirements for cooling, power supply etc.). The inner radius is determined by the radius of the beam pipe (3cm), the outer radius is limited by the TPC. Four innermost layers are silicon pixel and silicon drift detectors, because they are truly two-dimensional (density of the particles at this layers are up to $90cm^{-2}$). The last two layers are double-sided silicon microstrip detectors (particle density is below $1cm^{-2}$). SSDs and SDDs are capable to identify non-relativistic particles thanks to dE/dx measurement, so ITS can be used as low-p_t spectrometer. Particles with momentum below 100MeV/c will be detectable only with ITS.

Many factors were taken into consideration for the design of the ITS:

Acceptance - the pseudorapidity[1] coverage of the tracking system is $|\eta| < 0.9$. It is necessary for a good efficiency for large-mass particle decay detection. Thanks to full azimuthal coverage, rejection of low-mass Dalitz[2] decays should be effective. The first pixel layer has a wider pseudorapidity coverage, $|\eta| < 1.75$.

dE/dx - minimum of four measurements is necessary for application of truncated mean[3] method. This is why four of six layers have analog readout (SDDs and SSDs). Resolution, e.g., for kaons at 0.98GeV/c, is approximately 10.6% [12].

Material budget - amount of material in the active area must be as low as possible (suppression of multiple scattering). On the other hand, thickness of silicon detectors used to measure ionization densities must be large enough to ensure required signal-to-noise ratio.

[1]Pseudorapidity, the quantity approximately equal to rapidity, is defined:

$$\eta = -\ln \tan \frac{\nu}{2} \tag{4.1}$$

where ν is an angle of the fly out particle, relative to the beam.

[2]Decay of the electrically neutral pion into a photon and an electron-positron pair.

[3]Two highest pulse heights are discarded.

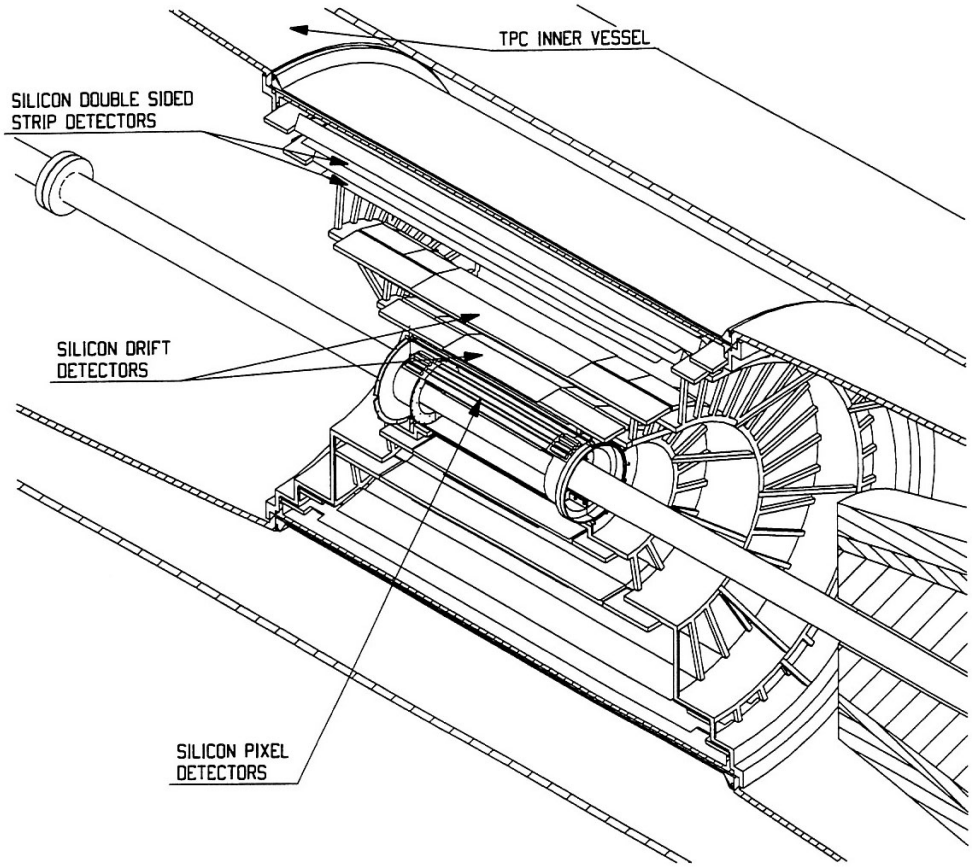

Figure 4.1: *General view of the ITS.*

This is important requirement for electronics, cabling, cooling system and support structure.

Granularity and spatial precision - granularity of the detector is determined by expected particle density. ITS is designed for track density of 8000 tracks (theoretical upper limit) per unit of rapidity, at midrapidity. Impact parameter for charmed particles must be better then $100\mu m$ in the φ direction, therefore, detectors have a spatial resolution few tens of μm (the best precision have detectors closest to the primary vertex - $12\mu m$). For detection of decay products from charmed mesons and high-mass quarkonia is necessary to measure particles with momenta over 3GeV/c, so the spatial precision becomes essential.

Radiation levels - Total dose during experiment lifetime was calculated from few krad (outer parts) to 150krad (inner parts). ITS is designed to withstand doses of ionizing radiation, expected during 10 years of activity.

Readout rate - Two different triggers, one trigger whole ALICE (centrality trigger), the other activates only SPD (muon arm trigger).

The geometrical dimensions and technical specifications are summarized in the table 4.2. The large number of channels in the ITS requires a large number of connections. However, minimum of material is needed, and so TAB bonded aluminium multilayer microcables (see section 5.5) are used instead of conventional copper cables. Front-end electronics and detec-

Layer	Detector	Cululated dose ($krad$)	Neutron fluence ($10^{11} cm^{-2}$)
1	pixel	130	3.2
2	pixel	39	3.1
3	drift	13	3.5
4	drift	5	3.3
5	strip	2	3.7
6	strip	2	3.3

Table 4.1: *Radiation dose and neutron fluence for each of the ITS detector layers, calculated for ten years of operation.*

Layer	Detector	r (cm)	$\pm$ z(cm)	Area (m^2)	Ladders	Tot. channels
1	pixel	4	16.5	0.09	80	5 242 880
2	pixel	7	16.5	0.18	160	10 485 760
3	drift	14.9	22.2	0.42	14	43 008
4	drift	23.8	29.7	0.89	22	90 112
5	strip	39.1	45.1	2.28	34	1 201 152
6	strip	43.6	50.8	2.88	38	1 517 568

Table 4.2: *Dimensions of the active areas of the ITS detectors.*

tors produce a large amount of heat which has to be removed (at preservation of temperature stability). This is important mainly for SDDs, which are sensitive to temperature variations in the 0.1K range. The outer four subdetectors are assembled onto a mechanical structure made of two end-cap cones connected with a cylinder between SSDs and SDDs. Both the cones and the cylinder are made of carbon-fibre and $Rohacell^{TM}$. SPDs are assembled in two half-cylinders, designed for safe installation around the beam pipe. The end-cap cones provide the cabling and cooling connection of subdetectors and the outside services. Now, I briefly describe SPD and SSD layers. SDD will be described more detailed in the next chapter (because this is the main topic of this thesis).

4.2 Silicon pixel detector

SPDs were chosen as two innermost layers of the ITS, because 2-D readout with geometrical precision, high speed and great double-hit resolution are needed so close to beam pipe . They will operate in a region where the track density is bigger than $50 cm^{-2}$ and a total radiation dose in 10 years is estimated to be approximately 200krad for the innermost layer. High segmentation leads to a low diode capacitance, resulting in an excellent signal-to-noise ratio. The price to pay for the use of detector with very high segmentation is a very large amount of connections and electronic channels. Basic building block of SPD is the ladder, consisting of a pixel detector matrix, flip-chip bonded (five-pitch surface packaging technique) to 8 front-end chips. The matrix consists of 256×256 cells, one cell measures $50 \mu m$ in the $r\varphi$ direction and $300 \mu m$ in the z direction. Four ladders are aligned in the z direction to a multilayer thin carrier (stave bus), which contains the bus and power lines. Two chips located at the ends

Parameter		Silicon Pixel	Silicon Drift	Silicon Strip
Spatial precision $r\varphi$	μm	12	38	20
Spatial precision z	μm	70	28	830
Two track resolution $r\varphi$	μm	100	200	300
Two track resolution z	μm	600	600	2400
Cell size	μm^2	50×300	150×300	95×40 000
Active area per module	mm^2	13.8×82	72.5×75.3	73×40
Readout channels per module		65 536	2×256	2×768
Total number of modules		240	260	1770
Total number of cells	M	15.7	34	2.7
Average occupancy (inner layer)	%	1.5	2.5	4
Average occupancy (outer layer)	%	0.4	1.0	3.3
Power dissipation in barrel	W	1500–2000	510	1100
Power dissipation end-caps	W	—	410	1500

Table 4.3: *Parameters of the various detector types.*

of the stave bus provided readout and control function and transmit the binary data to a remote router (via serial copper link). Six staves (2 from the inner layer and 4 from the outer layer) are mounted on a carbon fibre support and cooling sector. Ten such sectors make full barrel around the beam pipe. SPD is expected to generate about 2kW of heat. In order to avoid radiation of heat to SDD layers, an Al-coated carbon-fibre shield surrounds the SPD.

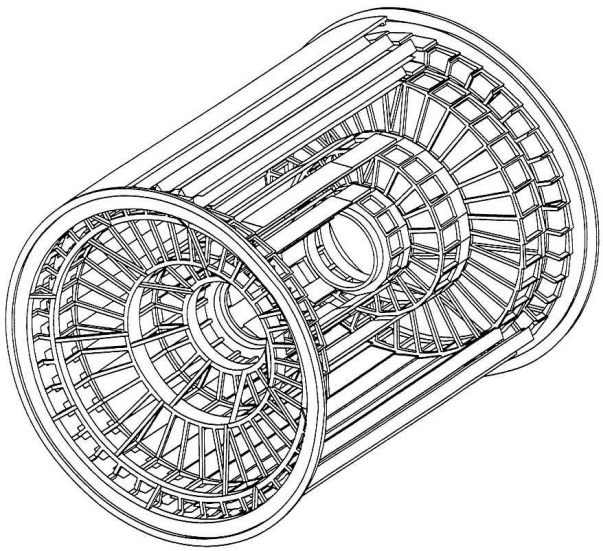

Figure 4.2: *The mechanical support of the ITS.*

4.3 Silicon strip detector

The two outer layers of the ITS consist of double-sided SSDs. Double-sided microstrips have been selected because they introduce less material in the active volume, than single-sided microstrips. SSDs are used in several experiments; can be produced in large quantities in

industry and are available with integrated resistors and capacitors. Ladders for the SSD layers are similar to carbon fibre ladders used in SDD layers, but are longer (120cm, 25g). The detectors mounted on the ladder overlap in the z direction and the ladders are mounted at two different radii, so SSDs overlap also in the $r\varphi$ direction. Since the SDD layers are sensitive to temperature gradients and temperature changes, SSD cooling system is designed to keep temperatures far below those needed for the strip detectors. As a medium for the cooling, a water is chosen.

Chapter 5

SDD of the ALICE

5.1 Overview

SDDs have been selected as third and fourth layer of the ITS, because they have a good multi-track capability and simultaneously provide dE/dx information.

Drift detectors measure transport time of the charge deposited by a traversing particle and reconstruct impact point (in one dimension) from this information. SDDs refine resolution at the cost of speed. This is very useful for experiments with low event rates and very high particle multiplicities.

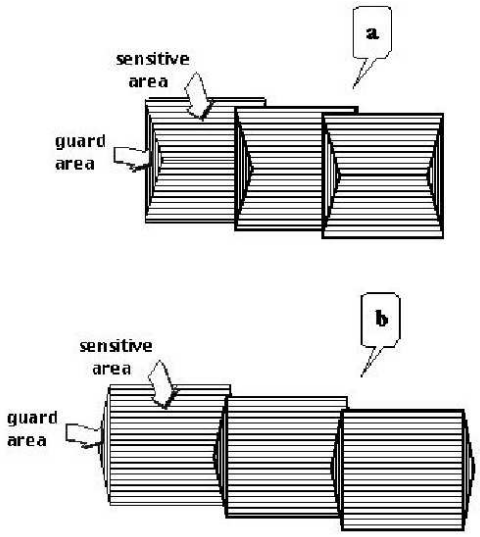

Figure 5.1: *Schematic illustration of adjacent SDDs in the ladder assembly. a) SDD prototypes with a classical 'butterfly geometry. b) final version of the detectors; their hexagonal shape minimizes the overlapping of adjacent SDDs'*

Detectors are mounted on linear structures - ladders, each holding 6 detectors for the third layer (radius 14.9cm) and 8 for the fourth layer (radius 23.8cm). Layers will be composed of 14 and 22 ladders, respectively. Each detector will be assembled with front-end electronics and power supply as a unit (called module), which will be tested and only then mounted on the ladder. The detectors overlap slightly (both in $r\varphi$ and in z), as can be seen in Fig. 5.1.

The front-end electronics, detectors and end of ladder are connected with TAB bonded Al microcables (see sec. 5.5). The design of the silicon drift detectors ran both in Italy and Řež (Czech Republic). SDD has a very strict requirement on the defects, which can appear during the lithographic process, so Neutron Transmutation Doped silicon (NTD) was chosen as a construction material. This material has a great homogeneity, because of the production process. Material suitable for production of SDDs have resistivity variations below 2%. During tests of prototype (performed in the years 1997–98) a new sort of MOS injection electrodes, capable to produce a spot-like charge clouds at the top of the drift region, was developed. It can serve as a tool of precise mapping of the drift speed across the detector (calibration of the drift time for temperature variations). In the electrostatic potential showed in Fig. 5.2, the charge cloud drifts with constant speed and carries the information of the coordinates of the impact point. Precision in determination of coordinates is better than $30\mu m$ and double

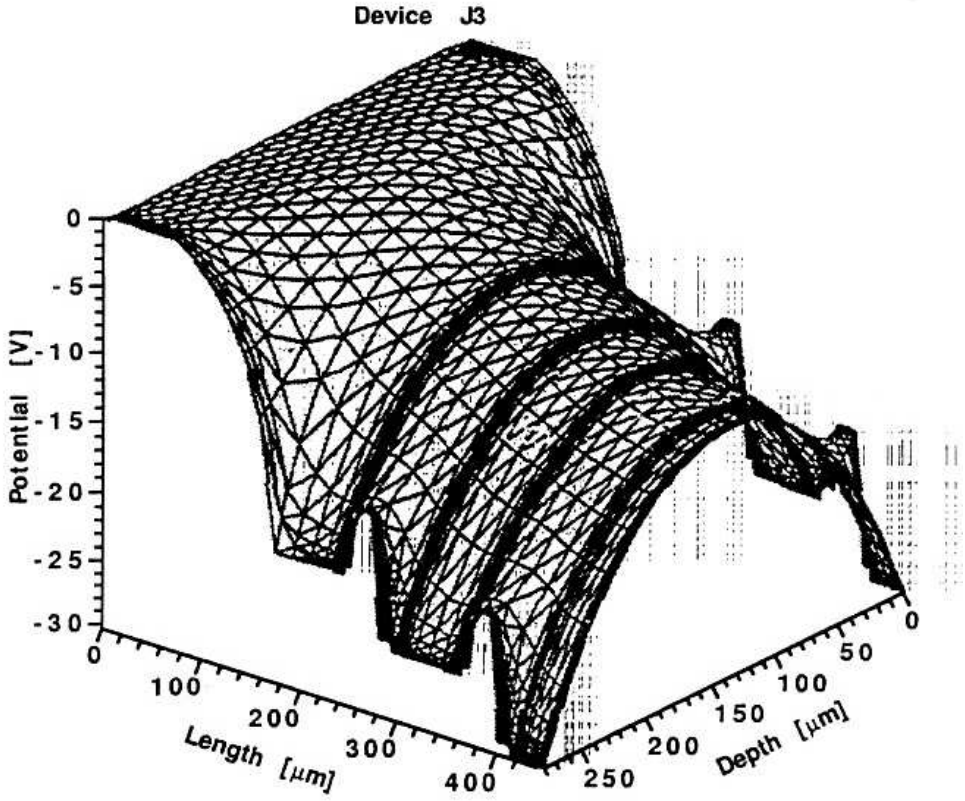

Figure 5.2: *Simulated shape of the electric field in a SDD.*

track resolution is better than $300\mu m$ (detailed information are in the table 4.3) In the linear SDD (see section 2.1), a series of parallel p^+ implant strips (drift cathodes) is placed on both sides of the detector, in the n-type silicon substrate. Drift cathodes fully deplete the volume and provide electrostatic field, forming a drift region. Minimization of the number of external connections is important, so the high-voltage divider (high-resistivity p^+ implantation was used as a divider) is integrated in the detector substrate. On board divider is supported by an external divider.

Guard cathodes serve to gradually scale the high potential of the drift cathodes to the ground

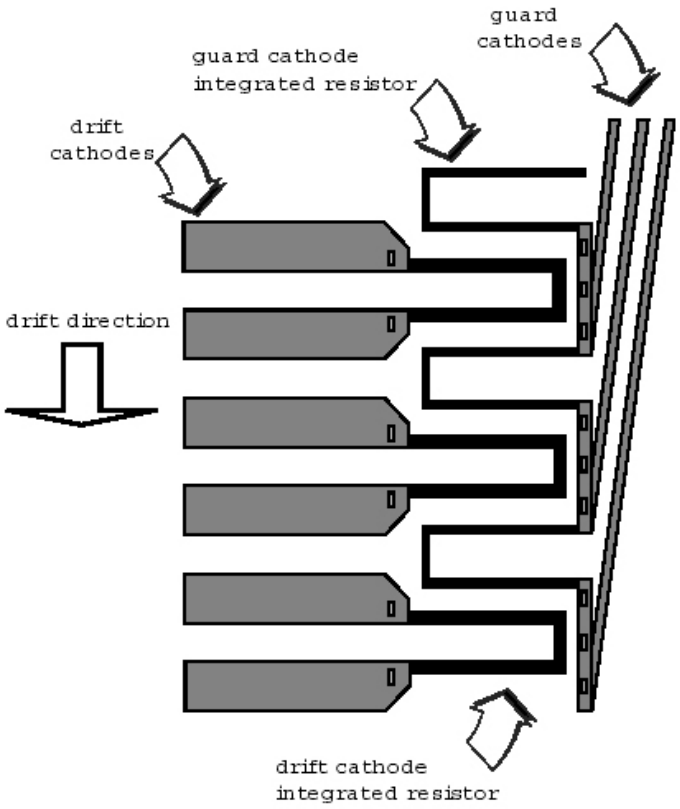

Figure 5.3: *Detail of the voltage dividers at the cathode and guard region of the ALICE-D1 detector.*

potential of the n^+ ring. Some of the last cathodes near the anodes serve to drive the drifting charges from the middle plane of the detector to the array of anodes (collection zone). The small size of anodes (small capacitance) implies low noise and good energy resolution. Electrons reach the anode region with a Gaussian distribution (owing to the mutual repulsion and diffusion during the drift).

5.2 Test results

Drift detector design, realized during 1998 (called ALICE-D1) [3] worked at field 600V/cm and has a drift speed about $8 \times 10^3 m/s$.

5.2.1 Determination of the hit position

In Fig. 5.4, there is the 2-D histogram of the time sample vs. the anode number, for typical 1-particle hit. Next to it, there is the memory content of individual channels. Identification of the charge clusters is following: First, individual channel outputs are analyzed. Hit is considered, if signal is higher than threshold level for two consecutive time segments and until it goes below the same threshold for two consecutive segments. If any two 1-D hits from neighboring anodes overlap in time, they are considered as component of one cluster. Then,

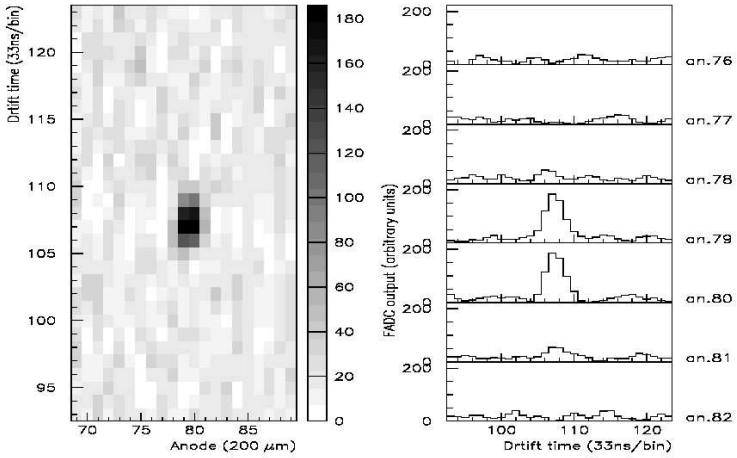

Figure 5.4: *Typical event display for a particle crossing the middle of the SDD. On the right the content of individual FADC channels is shown.*

the position of the center of gravity, total cluster charge, and other variables are calculated.

5.2.2 Efficiency of the detection

Amplitude of the signal in the SDD depends on the amount of deposited charge and on the drift time (because of diffusion). Dependence of the amplitude on drift time is inversive. Signal-to-noise ratio depends on the drift time (and drift time depends on the size of the electric field). Signal is well separated from the noise at highest field. Several sizes of the electric field (300V/cm, 460V/cm and 650V/cm) were examined in the time of testing ALICE-D1 prototype. For example, at field 460V/cm were detected all clusters up to 26mm drift length (in the sense of ratio between the number of tracks for which a cluster is detected in the SDD and reconstructed by the comparative microstrips). From these results was set electric field 600V/cm, ensured essentially 100% efficiency for the full drift length of 36mm.

5.2.3 Monitoring of the drift velocity

Drift velocity depends on mobility (1), and mobility is strongly affected by temperature:

$$\mu \propto T^{-2.4} \tag{5.1}$$

So it is needed to control temperature variations within 0.1K range, to ensure necessary resolution. Drift velocity monitoring is secured by charge injectors. In Fig. 5.5 are variations of the drift time and drift velocity during more than one day.

Fluctuations of velocity 55m/s correspond to 1.5K temperature variations. Drift velocity variations were measured and calculated by two methods - with injectors and with microstrips, and both give the same result (different $< 5\%$).

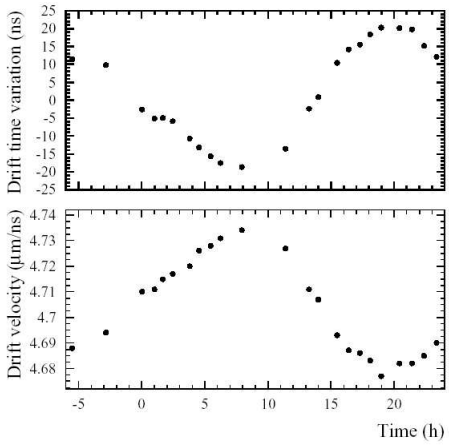

Figure 5.5: *Drift time variation (top) measured for injected charge and drift velocity (bottom) calculated using the microstrip telescope as a function of the time of day.*

5.3 Electronics

5.3.1 Overview

Choice of the drift electronics was done with respect to the two main requirements: very low power budget (because of temperature sensitivity of the SDDs) and low amount of material on the ladders (it restricts size of the cooling system and cabling). Each half-detector has 256 anodes and each anode 256 time samples, so amount of generated data is very large (and it dictates requirements for cabling). Because of these requirements, two-buffer front-end system has been designed. First buffer is a fast analog memory, second buffer is a static RAM. Data from SDD are continuously stored in the analog memory and transferred after ADC to the second buffer only after trigger signal (the required sampling frequency is 40MHz, it is almost impossible to design ADC at this speed with so small power budget - solution is just the analog memory and then digital conversion only after trigger signal). The second buffer can store several events, so it is possible to reduce the data. Zero suppression didn't get sufficient results, more complex algorithms have been studied (see section 5.4). Front-end electronics is organized in two units located on the ladder. First unit, which readouts 256 anodes contains preamplifier, analog buffer and ADC (this circuit is called PASCAL), second chip contains digital event buffers (AMBRA). The data compression (CARLOS architecture) and transmission are placed in two units at both ends of the ladder structure. Total radiation dose is expected low, but single event effects (requirement of the radiation-tolerant techniques) must be taken into the consideration.

5.3.2 Trigger

The trigger in the ALICE is organized into three different levels [4], L_0, L_1 and L_2, each with different latency. The reason for this separation is the different arrival times of the trigger inputs and timing requirements of the detectors. In some detectors, front-end electronics require a strobe early, so first decision must be delivered $1.2\mu s$ after collision (L_0 decision). Some trigger detectors are not able to send input in time, they act in the L_1 decision, which arrives at the detectors after $6.5\mu s$. Third step comes after the end of the drift time of the

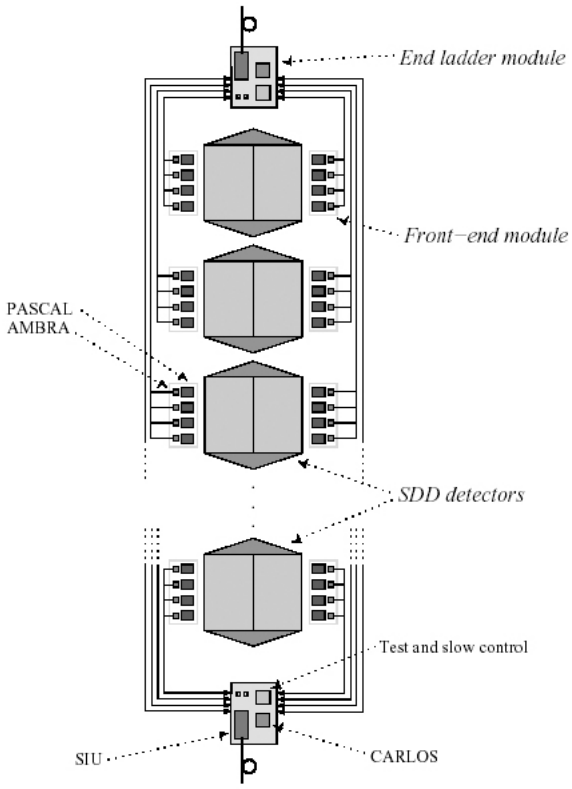

Figure 5.6: *The SDD ladder readout architecture.*

Signal Status	L_0 (μs)	L_1 (μs)	L_2 (μs)
Last trigger input at CTP	0.8	6.1	87.6
Trigger output at CTP	0.9	6.2	87.7
Trigger output at detector	1.2	6.5	88.0

Table 5.1: *Latencies associated with different trigger levels in the CTP.*

TPC (L_2 decision), at about $88\mu s$.

SDD readout system will behave in this way:

1. Starts the acquisition after an L_1 signal (absence of this signal means event rejected). The acquisition has to be delayed with respect to L_1 (total drift time must be taken into consideration).

2. Aborts the acquisition after L_{2_n} (in standard Pb-Pb mode, 95% of L_1 events will be rejected).

3. Replies to the trigger system within 1–1.3μs after L_0.

5.4 Data reduction

5.4.1 First data reduction

The main aim of the first data reduction is to reduce the number of bits per sample from 10 to 8. The principle is to decrease the resolution for larger signals with a square-root or logarithmic law. Since the larger signals have a better signal-to-noise ratio than the smaller ones, the precision of the measurement is not affected. This operation can be done with a nonlinear response preamplifier (it simplifies the design of the analog memory and ADC - they need 8-bit instead of 10-bit resolution).

5.4.2 End-ladder data reduction

There exist several ways:

1. Zero sequence encoding - sequences of zeros are transmitted as a zero code followed by a number of zeroes. This algorithm is very useful for systems with low occupancy.

2. Simple threshold zero suppression - the data below a certain value are set to zero.

3. Differential encoding - the difference between consecutive samples is transmitted, instead of the own values of samples.

4. Simple threshold tolerance - this is 3) and 2) applied consecutively.

5. Huffman encoding - This uses a variable length encoding (probability of lower codes is higher than that of higher ones). Huffman encoding is a lossless data reduction.

6. Multithreshold zero suppression - a sample is set to zero depending on its value and on the value of adjacent samples. Data losses are smaller than in the case 1).

5.5 Cabling

The cabling requirements are following: Connections between the front-end and the end-ladder electronics is a critical aspect of the SDD readout system, because the amount of material is critical in this region. Connections between the end-ladder units and the DAQ must be compatible with the ITS mechanical insertion. First cables will be assembled in the laboratory, second after the placement of the ITS (so easy-to-manage connectors have to be used).

Standard commercially available cable technology of TAB bonding ($Kapton^{TM}$ tape with copper strips formed by using a lithographic process) has several drawbacks: The soldering of copper wires with aluminum bonding pads requires much more energy and force than the standard bonding technique; copper increases the total amount of material in the detector area (by factor of three) - the ratio between radiation length and conductance is much better for Al than for Cu; the cost is also very relevant. So there was, within ALICE, developed technology which uses Al strips on a $Kapton^{TM}$ support.

Chapter 6

PCI to VME Interface

As a part of my thesis, I participated on building the testing apparatus for SDD AZTEC (see section 2.3). This apparatus will be used for R&D, education, and it is possible that it will also be used in the new experimental practical next year. My task was to start up the PCI-VMEbus interface for PC from W-Ie-Ne-R Plein & Baus GmbH [14]. Interface consists of VMEMM 6U VME Master, 32bit PCI Bus Interface card PCIADA, SCSI2 cable, CD with documentation (mostly in German) and software (out of date). The main idea is to use the PC, with help of the PCI-VME interface, instead a VME processor module. The PC development is extremely fast and we can profit from that.

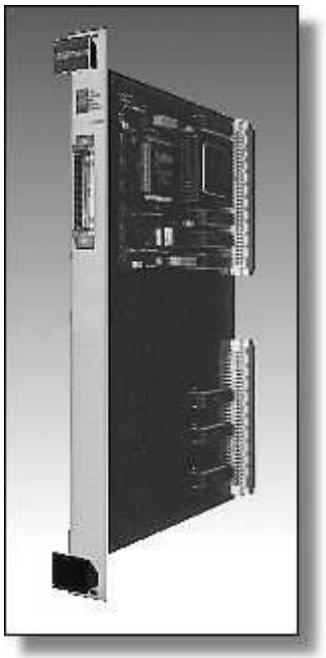

Figure 6.1: *VMEMM VME bus master*

I had no previous experience with such device (nor with programming). First I learned to program in the C language and how to work with the Linux operating system (this part took the most of time). I read the manual and tried to install the Linux drivers. I excluded two of three (arwvme 1.37 and arwvme 1.46), because they didn't match with the system (kernel 2.4.21) and I didn't manage to debug them. I installed the driver from Klaus Hitschler

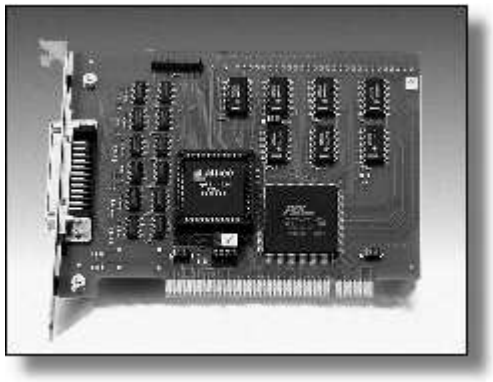

Figure 6.2: *PCIADA interface*

(ARW Elektronik Germany, 2002) and it seemed functional. The driver could read out some registers[1], for example INTCSR (Interrupt Control / Status Register), but was not able to do a RAM test (to write and then to read data from the VME memory area). For a long time I thought that I don't understand how to address the memory, but now I am convinced about disfuctionality of the driver. To solve this problem, I suggest to use a Windows 98 operating system (drivers on the CD from W-Ie-Ne-R are very old), or write an own driver (now I don't have enough knowledge).

My work on PCI-VME interface is at a deadlock, but I will continue in finding the solution. At the present time, I work on another device - computer controlled crate for SDD power sources from ISEG Spezialelektronik GmbH.

[1]At the boot time, pci-vme device gets several different memory areas:

- 54 Byte Local Configuration Register (LCR) of the I/O area. LCR contain different control status registers and base addresses
- LCR in the memory area
- 8 kByte of the memory area for direct access to VME and the local VMEMM memory area

Conclusion

Silicon drift detectors are relatively new, sophisticated semiconductor detectors. They provide very good 2-D resolution and, in comparison with e.g. silicon strip detectors, require less electronics and wiring. Silicon drifts combine good tracking capability and provide dE/dx information. The disadvantage of this detectors is a relatively low speed (in comparison with other semiconductor detectors) and great temperature sensitivity (this require efficient cooling and good monitoring of the drift velocity). SDDs are very useful in experiments with low event rates and high particle multiplicities, e.g. ALICE or STAR.

List of abbreviations

ADC	Analog to Digital Converter
ALICE	A Large Ion Collider Experiment
AMBRA	A Multievent Buffer Readout Architecture
CARLOS	Compression And Run Length encOding Subsystem
CTP	Central Trigger Processor
DAQ	Data AcQuisition
FADC	Flash Analog to Digital Converter system
FMD	Forward Multiplicity Detector
HMPID	High Momentum Particle IDentification
ITS	Inner Tracking System
LEP	Large Electron-Positron collider
LHC	a Large Hadron Collider
NTD	Neutron Transmutation Doped silicon
PASCAL	Preamplifier, Analog Storage and Conversion from Analog to digital
PHOS	PHOton Spectrometer
PID	Particle Identification Detector
QGP	Quark-Gluon Plasma
RHIC	a Relativistic Heavy Ion Collider
STAR	a Solenoidal Tracker at RHIC
TAB	Tape Automatic Bonding
TPC	Time Projection Chamber
TRD	Transition Radiation Detector
ZDC	Zero Degree Calorimeter

Bibliography

[1] L. Eckertová et al., Fyzikální elektronika pevných látek, Univerzita Karlova, Praha 1992.

[2] ALICE Collaboration, Technical Proposal, CERN/LHCC/95-71.

[3] ALICE Collaboration, Technical Design Report of the Inner Tracking System, CERN/LHCC/1999-12.

[4] ALICE Collaboration, Technical Design Report of the Trigger, Data Acquisition, High-Level Trigger and Control System, CERN/LHCC/2003-62.

[5] W. Chen et al., IEEE Trans. Nucl. Sci. NS-39 (1992) 619.

[6] E. Gatti et al., Nucl. Instr. Meth. A274 (1989) 469.

[7] A. Castoldi et al., Nucl. Instr. Meth. A399 (1997) 227.

[8] P. Řehák et al., Nucl. Instr. Meth. A377 (1996) 367.

[9] P. Řehák et al., Spiral silicon drift detectors, IEEE Nuclear Science Symposium, 1988.

[10] J. Gerndt, Detektory ionizujícího záření, Vydavatelství ČVUT, Praha 1994.

[11] Official webpages of the ALICE Collaboration http://aliceinfo.cern.ch

[12] H. Yamamoto, dE/dx Particle identification for Collider detectors, http://hep45.hep.colostate.edu/∼wilson/flc/talks/dEdx-wrup-Yamamoto.pdf

[13] Z. Doležal, Polovodičové detektory v jaderné a subjaderné fyzice, http://www-ucjf.troja.mff.cuni.cz/∼dolezal/teach/semicon/semi_p.pdf

[14] manual and software to the PCI-VMEbus Interface for PC from W-Ie-Ne-R Plein & Baus GmbH.